

# A Study of Quasar Radio Emission from the VLA FIRST Survey

Yogesh Wadadekar,<sup>1</sup> and Ajit Kembhavi <sup>2</sup>

Inter University Centre for Astronomy and Astrophysics, Post Bag 4, Ganeshkhind, Pune 411007,  
India

## ABSTRACT

Using the most recent (1998) version of the VLA FIRST survey radio catalog, we have searched for radio emission from 1704 quasars taken from the most recent (1993) version of the Hewitt and Burbidge quasar catalog. These quasars lie in the  $\sim 5000$  square degrees of sky already covered by the VLA FIRST survey. Our work has resulted in positive detection of radio emission from 389 quasars of which 69 quasars have been detected for the first time at radio wavelengths. We find no evidence of correlation between optical and radio luminosities for optically selected quasars. We find indications of a bimodal distribution of radio luminosity, even at a low flux limit of 1 mJy. We show that radio luminosity is a good discriminant between radio loud and radio quiet quasar populations, and that it may be inappropriate to make such a division on the basis of the radio to optical luminosity ratio. We discuss the dependence of the radio loud fraction on optical luminosity and redshift.

*Subject headings:* quasars: general— methods: statistical— catalogs— surveys

## 1. INTRODUCTION

It has been well known for some time that only about 10% of quasars are radio loud, with radio luminosity comparable to optical luminosity. This is surprising, because over a very wide wavelength range from  $100\text{ }\mu\text{m}$  through X-ray wavelengths, the properties of radio loud and radio quiet quasars are very similar. The presence or absence of a radio component may be a pointer to different physical processes occurring in the two types of quasar, but it is not yet clear as to what these processes are.

The relationship between quasar radio and optical emission was initially studied using radio selected objects, which generally had high radio luminosities because the early radio surveys had relatively high limiting radio fluxes. Sandage (1965) showed that not all quasars are powerful radio emitters, and that a substantial population of *radio quiet* quasars exists, undetectable at

---

<sup>1</sup>yogesh@iucaa.ernet.in

<sup>2</sup>akk@iucaa.ernet.in

high radio flux levels. Since then, in addition to radio surveys, radio follow up observations of large surveys conducted in the optical have been used to study the radio properties of quasars (eg. Sramek & Weedman 1980; Condon *et al.* 1981; Marshall 1987; Kellerman *et al.* 1989; Miller, Peacock & Mead 1990). Such targeted radio observations, of quasars selected by other means, typically go deeper than the large radio surveys, as a result of which the median radio luminosity of these samples is lower. Taken together, these two survey methods have detected quasars with a range of more than 6 orders of magnitude in radio luminosity, but the populations detected by the two methods come from different regions of the overall radio luminosity distribution.

The radio emission from quasars can be used to divide them into two classes: a radio loud population where the ratio  $R$  of radio to optical emission is greater than some limiting value  $R_{\text{lim}}$  and a radio quiet population with  $R < R_{\text{lim}}$ . Such a separation is commonly employed in the literature dealing with the radio properties of quasars, with  $R_{\text{lim}} = 1$  or  $R_{\text{lim}} = 10$  (eg. Kellerman *et al.* 1989; Visnovsky *et al.* 1992; Stocke *et al.* 1992; Kellerman *et al.* 1994). Alternately, the separation between radio loud and radio quiet quasars, may be defined by their radio luminosity. Such a criterion has been advocated by Miller, Peacock & Mead (1990), who noticed that for a sample of optically selected quasars, which spanned a wide range of optical luminosity but a narrow range of redshift, there was no correlation between their optical and radio luminosity. This implied that the distribution of  $R$  was optical luminosity dependent, thus making it unsuitable as the discriminant between radio loud and radio quiet populations. Miller *et al.* found that the distribution of radio luminosity was highly bimodal, and from an examination of the luminosities of radio detections and upper limits accepted a 5 GHz limiting radio luminosity of  $10^{25} \text{ W Hz}^{-1} \text{ str}^{-1}$  (we use  $H_0 = 50 \text{ km sec}^{-1} \text{ Mpc}^{-1}$ ,  $q_0 = 0.5$ , quasar radio spectral index  $\alpha_r = 0.5$  and optical spectral index  $\alpha_{\text{op}} = 0.5$  throughout this paper) as the dividing line between radio loud and radio quiet quasars.

The gap in the radio luminosity function of the two populations is pronounced, with very few objects occupying the region between quasars that are radio loud and those that are radio quiet. The detection technique used to find quasars from these two populations are also different. An overwhelming majority of radio loud quasars have been first detected in the radio and then confirmed using optical spectroscopy, while radio quiet quasars have been detected using optical, X-ray or other techniques. An important question in such a situation is: are radio quiet and radio loud quasars indeed two physically different populations, or is the distinction merely an artifact caused by selection biases in the detection techniques? Previous efforts at answering this question have been plagued by the small size of the datasets and their incompleteness. Most radio observations of optically selected quasars have lacked the sensitivity to detect their radio emission. There have been a few high sensitivity radio surveys (eg. Hooper *et al.* 1996, Kukula *et al.* 1998) but the size of their samples is quite small. The VLA *Faint Images of the Radio Sky at Twenty centimeters* (FIRST) survey (Becker *et al.* 1995; for more upto date information see the FIRST survey homepage at <http://sundog.stsci.edu/>) allows us to address this question meaningfully, by combining a large sky coverage with a low flux limit of 1 mJy at 20 cm. This ongoing survey, when

completed will cover 10,000 square degrees around the North Galactic Cap, the same area of the sky to be surveyed by the Sloane Digital Sky Survey (SDSS; <http://www.sdss.org/>). To date, data for approximately one half of the eventual sky coverage have been released.

FIRST allows us to address the issue of quasar bimodal radio luminosity distribution in two different but complementary ways. Firstly, optical identifications of FIRST sources using large optical surveys such as the Palomar Observatory Sky Survey (POSS) provide a large database of quasar candidates, whose true nature can then be verified spectroscopically. Several such efforts (eg. Gregg et al 1996; Becker *et al.* 1997) are currently underway. Secondly, the large area covered by the FIRST survey allows us to look for radio emission from a significant fraction of already known quasars and correlate their radio properties with other observables. In the present paper, we have used this approach to determine the radio properties of quasars from the catalog of Hewitt & Burbidge (1993, hereafter HB93).

Such an approach has also been taken, though with a different radio survey and quasar catalog, by Bischof and Becker (1997, hereafter BB97) who compared positions of radio sources from the NVSS radio survey (Condon *et al.* 1998), with the positions of 4079 quasars from the Veron catalog (Veron-Cetty and Veron 1991). They detected radio emission from 799 quasars, of which 168 were new radio detections.

The FIRST survey has better sensitivity and resolution than the NVSS, but covers a smaller area. There is a small area of overlap between NVSS and FIRST. The FIRST survey, which is being carried out with the VLA in its B-configuration, has excellent astrometric accuracy of  $\sim 1''$  (90% error circle) and a 5 sigma sensitivity of  $\sim 1$  mJy. This compares favorably with the D-array NVSS, which has a beam size of 45 arcsec and a 5 sigma sensitivity of  $\sim 2.4$  mJy. FIRST has a smaller beam size than NVSS, and so it is expected to have better sensitivity to point sources. We look for radio emission from the 1704 quasars from HB93 ( $\sim 23\%$  of the quasars listed therein) which lie in the area covered by the FIRST survey. This set of quasars is not statistically complete in any sense. Wherever appropriate, we distinguish between radio selected quasars and those selected by other means.

## 2. RADIO/OPTICAL COMPARISONS

We compare the positions of quasars in HB93 to the positions of radio sources in the FIRST radio source catalog (February 4, 1998 version available at <http://sundog.stsci.edu/>), and calculate the angular separation between each quasar and each FIRST source. About 4% of sources in the FIRST catalog have been tagged as possible sidelobes of bright sources. Of these,  $<10\%$  are real sources and considerably less than 1% of the unflagged sources in the catalog are sidelobes (White *et al.* 1997). We have excluded these flagged sidelobe sources from our cross correlation. We are then left with a total of 421,447 unflagged sources in the northern and southern strips, covering a total area of about 4760 square degrees. Of these, 368,853 sources lie in the northern strip while

52,594 sources are in the southern strip. On an average, there are 88.54 FIRST sources per square degree of sky.

Our quasar sample consists of 1704 quasars from HB93, that lie in the area covered by FIRST. We have excluded the BL Lacs listed in the catalog from the present work. In HB93, the authors use a simple selection criterion for quasars. Any object that is starlike (with or without fuzz) and has redshift  $z \geq 0.1$  is called a quasar; and is included in the catalog. The positions listed in the catalog are for the optical object, most of which are taken from the identification paper or from the paper containing the redshift measurement. If a quasar is very close to a bright galaxy, and the quasar coordinates are not available in the literature, the galaxy coordinates have been listed by HB93 for the quasar position.

In Figure 1 we show the distribution of the HB93 quasars on the sky in galactic coordinates. The apparent clustering of known quasars is due to the limited solid angle covered by deep quasar surveys (most of them optical) that have uncovered the largest number of quasars. The approximate area for which FIRST survey data has been released is also marked in the figure. FIRST has currently covered an area of 4150 square degrees around the North Galactic Cap in addition to two narrow strips totaling about 610 square degrees near the South Galactic Cap. The southern strip has a peculiar shape and the box shown here is a very approximate representation. Detailed sky coverage maps are available at the FIRST homepage.

In order to find coincidences between HB93 and FIRST sources, we begin with a search circle of radius  $300''$  centered on each HB93 quasar, and look for FIRST radio sources within this circle. When there is more than one FIRST source in the search circle, we tentatively accept all such sources as matches. In Figure 2 we show a histogram of the angular separation between the HB93 quasars and the FIRST sources found in the search circles.

The angular auto correlation function for FIRST has shown that 35% of sources have resolved structure on scales from 2–30 arcsec (Cress et al. 1996). Since our aim in this work is to only look for radio emission from the compact (flat spectrum) component of quasars, we have considered only quasars which contain at least one FIRST source within 10 arcsec of them. This would make us miss out on some quasars which may have elaborate extended radio structure, but a core emission lower than the FIRST flux limit. To see which of the radio sources found can be accepted as true identifications, we estimate the quasar–FIRST source chance coincidence rate for a random distribution of FIRST survey sources. For a random distribution, the chance coincidence rate is directly proportional to the area of sky covered by the search circle around each quasar, ie, the square of the search radius. The straight line in Figure 2 is the expected number of chance coincidences between quasars and FIRST sources, in annuli of radius shown on the abscissa and width 5 arcsec around the quasars. It is seen from the figure that the expected number of chance coincidences closely matches the number of actual coincidences beyond about 40 arcsec, indicating that most FIRST sources found more than 40 arcsec away from a quasar are chance coincidences. On the other hand, matches within 10 arcsec are mostly real (less than 1% chance identification

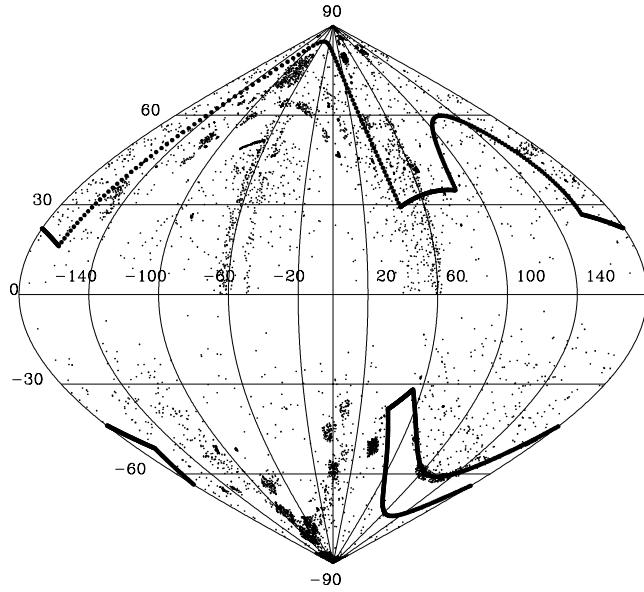


Fig. 1.— The approximate boundaries, in galactic coordinates, of the areas covered by the FIRST survey are indicated by bold points. The northern and southern strips are separately shown. The dots indicate quasars from the Hewitt and Burbidge (1993) catalog.

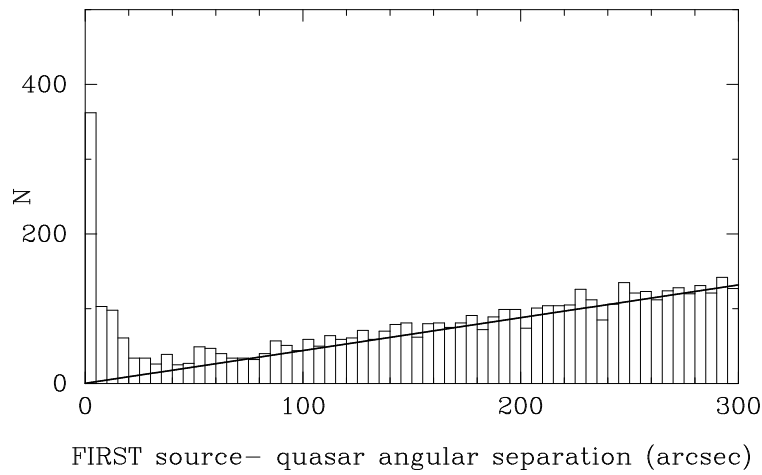


Fig. 2.— A histogram of the angular separation between the Hewitt and Burbidge (1993) quasars and the corresponding FIRST source. The straight line is the number of chance matches expected, for a search area of radius shown on the X-axis, if the FIRST sources were randomly distributed in the sky.

probability).

We therefore choose a search circle of radius 10 arcsec and count all matches found within this radius as true matches. All subsequent discussion about the radio properties of quasars only uses matches obtained with this search radius.

The positions of quasars listed in HB93 have astrometric errors of a few arcseconds or more in some cases. In such cases, there will be missed matches when the positional error places a HB93 quasar outside the 10 arcsec search radius around the FIRST radio source with which it is actually associated. Some of these missed can be recovered by using the accurate positions of star like objects from the USNO-A2.0 catalog (Monet *et al.* 1996), which is an all sky astrometric and photometric catalog of over 500 million starlike objects. For this purpose we considered FIRST radio sources which had a HB93 quasar in an annulus of inner radius 10 arcsec and outer radius 20 arcsec around it. We cross correlated the positions of such radio sources with starlike sources from the USNO-A2.0 catalog. The search radius used for this purpose was of 3 arcsec, which is three times the RMS uncertainty in the first survey positions (the positions in USNO-A2.0 are known to better than this accuracy). When an USNO-A2.0 object is found in this circle we compare its blue magnitude with the blue magnitude of the corresponding HB93 quasar. When the difference  $\delta m$  was less than one magnitude, we considered the USNO-A2.0 object and the HB93 quasar to be the same object.

We have a total of 158 FIRST sources with a HB93 quasar within the 10-20 arcsec annulus around it. Out of these 158 sources, 16 had a USNO-A2.0 source within a 3 arcsec circle around it, and of these 8 had blue magnitudes which passed our criterion. We accepted the corresponding 8 HB93 quasars as valid matches with FIRST survey sources, and added these to our list of 381 radio detections mentioned above.

We find that positions of radio selected quasars match the FIRST source positions better than the non-radio selected quasars. This is because the radio positions have been more accurately determined than optical positions. Accurate astrometry on optically selected quasars is often not available and quasar positions are computed approximately using finding charts. The mean astrometric error, in non-radio selected quasar surveys, is typically a few arcseconds. In high resolution radio selected surveys, the astrometric error is often less than an arcsecond. About 12% of quasars detected have more than one (usually two) FIRST sources within the search circle of 10 arcsec radius. In such cases, we have used *all* the FIRST sources associated with the quasar in our analysis. This is because generally the combined error in quasar and FIRST source positions is too large to allow us to reliably determine which of the two radio sources actually corresponds to the quasar core. There are  $\sim$ 1320 non detections, amongst the HB93 quasars covered by FIRST, and we assign an upper limit of 1 mJy to their radio flux at 1.4 GHz.

Table 1 provides a summary of our radio detections. The radio and optical properties of the quasars with FIRST detections (which includes all the new detections in the radio) are summarized in Table 2. Detections in the radio reported after the quasar catalog was published (mostly in

BB97) are mentioned in the last column. Those quasars which do not have the letter R in the selection technique code and do not have a recent radio detection mentioned in the last column may be considered to be the new detections. There are 69 such quasars in Table 2. The last eight entries are the additional list of matches obtained using a correlation with the USNO-A2.0 catalog. These 8 matches were obtained using an indirect comparison technique, and have *not* been used in the statistical correlations reported in subsequent sections.

### 2.1. 1343+266: not a gravitationally lensed quasar?

This is a close pair of quasars with identical redshift, similar spectra and separated by only  $\sim 10$  arcsec. Detailed spectroscopic observations have shown qualitative (eg. presence of certain lines) as well as quantitative (eg. ratio of line strengths) *differences* between the two quasars, strengthening the claim that this is *not* a gravitationally lensed pair, but a physically associated pair of quasars, possibly residing in a cluster of galaxies at  $z = 2.03$  (Crampton *et al.* 1988; Crots *et al.* 1994). The optical luminosities are comparable, with 1343+266B having a luminosity higher by about 5% than 1343+266A. We find radio emission from only one of the quasars: 1343+266B has a flux of 8.9 mJy. The separation between the gravitationally lensed quasar and the FIRST source is 2.18 arcsecond, which is consistent with an error of  $\sim 1''$  each in the quasar optical position and the FIRST radio position. There is no radio emission associated with 1343+266A at the FIRST flux limit of 1 mJy, because the FIRST source associated with 1343+266B is 7.4 arcsec away, too far to be associated with 1343+266A, considering the extremely accurate astrometry done for this well studied pair of quasars. There is no other FIRST source associated with 1343+266A. This implies that the radio luminosity of 1343+266B is at least 8.9 times higher than that of 1343+266A, in sharp contrast to only 5% difference in their optical luminosity. Such radio detection is strong evidence that the pair is *not* gravitationally lensed.

## 3. RADIO AND OPTICAL PROPERTIES

### 3.1. Bivariate luminosity functions

The number of quasars with optical luminosity in the range  $(L_{\text{op}}, L_{\text{op}} + dL_{\text{op}})$ , radio luminosity in the range  $(L_{\text{r}}, L_{\text{r}} + dL_{\text{r}})$  and redshift in the range  $(z, z + dz)$  is in general given by  $\Phi(L_{\text{op}}, L_{\text{r}}, z)dL_{\text{op}}dL_{\text{r}}dv(z)$ , where the *luminosity function*  $\Phi(L_{\text{op}}, L_{\text{r}}, z)$  is the comoving number density of quasars for unit ranges of the respective luminosities, and  $dv(z)$  is a comoving volume element at  $z$ . If the radio and optical luminosities are independently distributed, it is possible to separate the luminosity function as

$$\Phi(L_{\text{op}}, L_{\text{r}}, z)dL_{\text{op}}dL_{\text{r}}dv(z) = \Phi_{\text{op}}(L_{\text{op}}, z)dL_{\text{op}}dv(z)\Phi_{\text{r}}(L_{\text{r}})dL_{\text{r}}. \quad (1)$$

In this case there will be no correlation between the optical and radio luminosities of the quasars described by Equation 1.

Another form of the bivariate luminosity function extensively considered in the literature has been

$$\Phi(L_{\text{op}}, L_{\text{r}}, z) dL_{\text{op}} dL_{\text{r}} dv(z) = \Phi_{\text{op}}(L_{\text{op}}, z) dL_{\text{op}} dv(z) \Phi_{\text{R}}(R) dR, \quad (2)$$

where

$$R = \frac{L_{\text{r}}}{L_{\text{op}}} = \frac{F_{\text{r}}}{F_{\text{op}}} (1+z)^{\alpha_{\text{r}} - \alpha_{\text{op}}} \quad (3)$$

and  $F_{\text{op}}$  and  $F_{\text{r}}$  are the optical and radio flux densities at some fiducial points in the spectrum, which we will take to be at 2500Å and 5 GHz respectively. Since we take  $\alpha_{\text{op}} = \alpha_{\text{r}} = 0.5$ , the ratio of the luminosities is simply equal to the ratio of the fluxes. It is assumed here that the distribution of  $R$  is independent of the other variables. This form of the luminosity function was first introduced by Schmidt (1970) to describe the bivariate luminosity distribution of 3CR radio quasars. For a given optical luminosity  $L_{\text{op}}$ , it follows from Equation 3 that the radio luminosity ranges from  $R_{\text{min}} L_{\text{op}}$  to  $R_{\text{max}} L_{\text{op}}$  for  $R$  in the range  $R_{\text{min}} < R < R_{\text{max}}$  and the mean radio luminosity is given by

$$\langle L_{\text{r}} \rangle = \langle R \rangle L_{\text{op}}, \quad \langle R \rangle = \int_{R_{\text{min}}}^{R_{\text{max}}} R \Phi_{\text{R}}(R) dR, \quad (4)$$

with the function  $\Phi_{\text{R}}(R)$  being normalized to unity. The luminosity function in Equation 2 therefore implies that the mean radio luminosity increases with the optical luminosity.

In the following sections we will see whether the data from the FIRST survey is consistent with either of the two forms of luminosity function. In our discussion, we will use the following nomenclature to refer to different classes of quasars:

- RSQ: Radio selected quasars,
- OSQD: non-radio (mostly optical) selected quasars detected by FIRST,
- OSQU: optically selected quasars with radio upper limits.

The OSQD and OSQU include a few X-ray selected quasars, but their numbers are too small to warrant separate treatment. All radio selected quasars lying in the area covered by FIRST have radio emission higher than the FIRST limit of 1 mJy.

We have shown in Figure 3 the variation of absolute magnitude with redshift for all the quasars in our sample. In this figure, triangles represent RSQ while the OSQD are represented by open circles and the OSQU by dots. The optical luminosity of the sample ranges over  $\sim 4$  orders of magnitude, and the redshift goes upto  $\sim 3.6$ . All three kinds of quasar are distributed over much of these wide ranges.

### 3.2. Distribution of radio luminosity

The radio-selected quasars (RSQ) in our sample have all been discovered in radio surveys with flux limits much higher than the 1 mJy limit of the FIRST survey. For a given redshift, these quasars will have much higher radio luminosity than most of the non-radio selected component of our population. The radio luminosity distribution of the RSQ is consequently not representative of the distribution for the overall quasar population. We shall therefore omit the RSQ from the following considerations, except where they are needed in some specific context.

We have shown in Figure 4 a plot of the 5 GHz radio luminosity against redshift for non-radio selected quasars. The OSQD are shown as unfilled circles, while the OSQU are shown as dots, and form the almost continuous lower envelope which indicates the radio luminosity corresponding to a radio flux of 1 mJy over the redshift range. In Figure 5 is shown a plot of the 5 GHz radio luminosity against the absolute blue magnitude for the non-radio selected quasars. In this figure too, radio detections are shown as open circles, and the radio upper limits as dots. There appears to be a correlation between the logarithm of the radio luminosity and absolute magnitude, in spite of the large scatter in radio luminosity for a given absolute magnitude. The linear correlation coefficient for the 135 radio detections alone is 0.22, which is significant at the > 99.9 percent confidence level. However, it is seen from Figure 3 and Figure 4 that mean radio as well as optical luminosity increase with redshift, which is due to the existence of a limiting radio flux and apparent magnitude in the surveys in which quasars are discovered. A situation can arise in which an observed correlation between radio luminosity and absolute magnitude is mainly due to the dependence of each luminosity on the redshift  $z$ . It is important to see if the correlation remains significant when such an effect of the redshift on the observed correlation is taken into account. This can be done by evaluating a *partial linear correlation coefficient* as follows (Havilcek & Crain 1988; Kembhavi & Narlikar 1999).

Let  $r_{L_r, M}$ ,  $r_{L_r, z}$  and  $r_{M, z}$  be the correlation coefficients between the pairs  $\log L_r$  and  $M$ ,  $\log L_r$  and  $z$ , and  $M$  and  $z$  respectively. The partial linear correlation coefficient is then defined by

$$r_{L_r, M; z} = \frac{r_{L_r, M}^2 - r_{L_r, z} r_{M, z}}{\sqrt{1 - r_{L_r, z}^2} \sqrt{1 - r_{M, z}^2}} \quad (5)$$

The partial correlation correlation coefficient has the same statistical distribution as the ordinary correlation coefficient and therefore the same tests of significance can be applied to it. A statistically significant value for it means that the luminosities are correlated at that level of significance even after accounting for their individual dependence on the redshift.

For our sample of 135 radio detections, the partial linear correlation coefficient is 0.09, which is significant only at the 72 percent confidence level. The observed correlation between the radio luminosity and absolute magnitude thus appears to be largely induced by the effect of the large range in redshift over which the sample is observed. The lack of correlation found here is consistent with the results of Miller, Peacock and Mead (1990, hereafter MPM90) and Hooper *et al.* (1995).

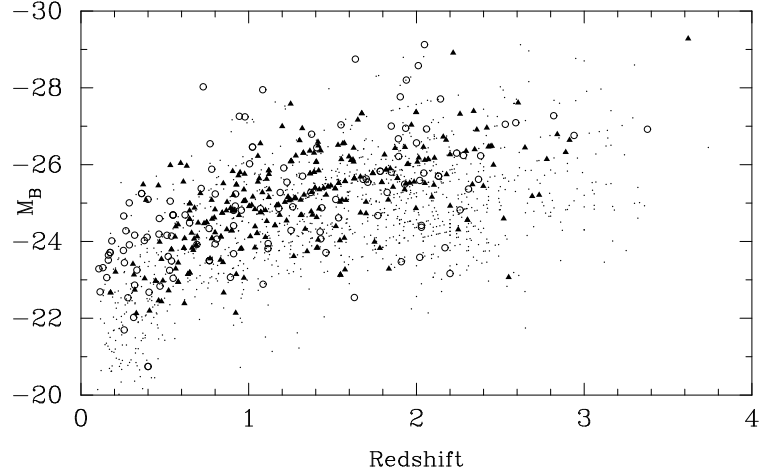


Fig. 3.— Absolute magnitude of quasars in our sample as a function of redshift. Non-radio selected (mostly optical) quasars with FIRST detection are indicated by open circles, solid triangles indicate radio selected quasars. The upper limits are represented by dots.

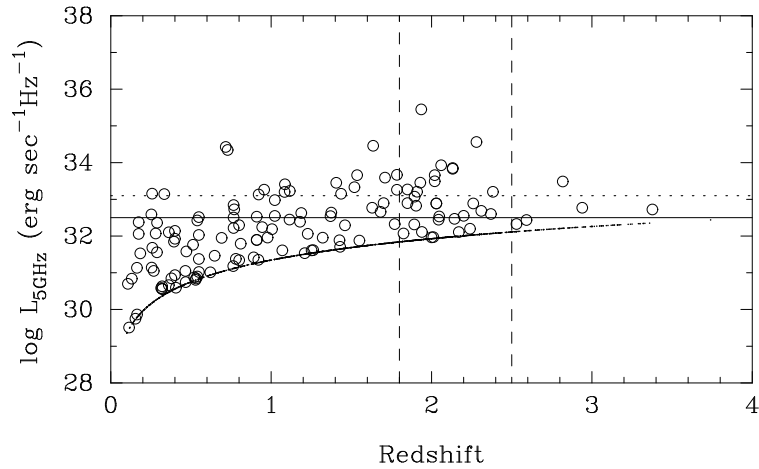


Fig. 4.— Radio luminosity as a function of redshift. The locus of dots indicates the 1 mJy upper limits. The horizontal dotted line is the dividing radio luminosity between radio loud and radio quiet objects adopted by MPM90. The solid horizontal line is the dividing luminosity that we have chosen. The region of redshift space explored by MPM90 is between the two vertical dashed lines.

MPM90 have observed a sample of optically selected quasars, with redshift in the range  $1.8 < z < 2.5$ , with the VLA to a limiting sensitivity of  $\sim 1$  mJy at 5 GHz. They detected nine quasars out of a sample of 44; these objects are shown in Figure 5 as filled squares. The radio upper limits of MPM90 occupy the same range as our upper limits shown in the figure, and are not separately indicated. MPM90 have commented at length on the luminosity gap found between their radio detections and upper limits. They concluded that the gap was indicative of a bimodality in the distribution of radio luminosity, which divides quasars into a radio loud population, with radio luminosity  $> 10^{25}$  W Hz $^{-1}$  str $^{-1}$ , and a radio quiet population with luminosity  $< 10^{24}$  W Hz $^{-1}$  str $^{-1}$ . The radio loud quasars were taken to be highly luminous representatives of the population of radio galaxies, and the radio quiet population was taken to be like Seyfert galaxies. The conspicuous gap between radio detections and upper limits is absent in our data. It is seen in Figure 5 that the region  $\sim 10^{32} \lesssim L_r(5 \text{ GHz}) \lesssim 10^{33}$  erg sec $^{-1}$  Hz $^{-1}$  (which corresponds to the gap found by MPM90 for our units and constants) is occupied by many quasars. Only seven of these are in the redshift range of the MPM90 sample, which probably explains why they did not find any quasars in the gap: our sample is about 30 times larger, and even then we find only a small number in the range.

In Figure 6 we show the distribution of the log of radio luminosity for the RSQ, the OSQD and the OSQU. The mean value for each is indicated by an arrow. The radio luminosity of the OSQD has a mean value of  $10^{32.24}$  erg sec $^{-1}$  Hz $^{-1}$ ), which is approximately 1.5 orders of magnitude fainter than the mean luminosity of the RSQ, because the latter were selected in high flux limit surveys. The RSQ have a median radio flux of  $\sim 400$  mJy, while there are only three OSQD with radio flux  $\geq 100$  mJy. The radio luminosity upper limits of the OSQU are well mixed with the fainter half of the luminosity distribution of the OSQD. The rather sharp cutoff in the luminosity upper limit distribution of the OSQU is due to the flattening in the 1 mJy luminosity envelope in Figure 4 at high redshifts. The upper limits peak at a luminosity which is approximately half a decade lower than the peak in the luminosity distribution of the OSQD. The mean value for the OSQU is  $10^{31.55}$  erg sec $^{-1}$  Hz $^{-1}$ . A Kolmogorov-Smirnov test on the distribution of radio luminosity of the OSQD and OSQU shows that they are drawn from different distributions with a significance of 99.9 percent. This is consistent with a bimodal distribution amongst the radio detections and upper limits. If the radio luminosity distribution is indeed bimodal, the present radio upper limits, when observed to a limiting flux significantly less than 1 mJy, would be found to have radio luminosities considerably lesser than the present set of detections.

### 3.3. Distribution of radio-to-optical luminosity ratio $R$

The ratio  $R$  is defined using rest frame monochromatic radio and optical luminosities at some fiducial rest frame wavelengths. In the following we will choose these to be at 5 GHz and 2500 Å in the radio and optical case respectively. With our choice of spectral indices  $\alpha_r = \alpha_{op} = 0.5$ ,  $\log R$  is given in terms of observed flux densities at observed wavelengths at 5 GHz and 2500 Å by

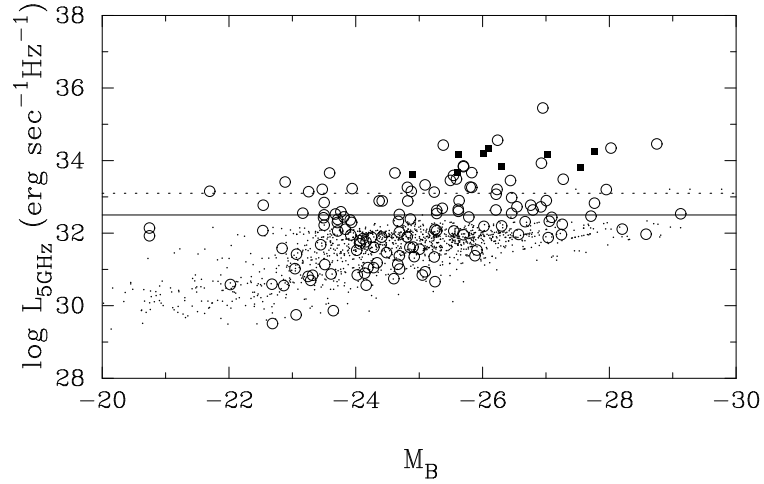


Fig. 5.— Radio luminosity as a function of absolute magnitude. The filled squares are radio detections of quasars studied in MPM90. The other symbols are as in Figure 4. The dotted horizontal line is the MPM90 dividing luminosity between radio loud and radio quiet quasars, in our units. The solid horizontal line is the dividing luminosity that we have chosen.

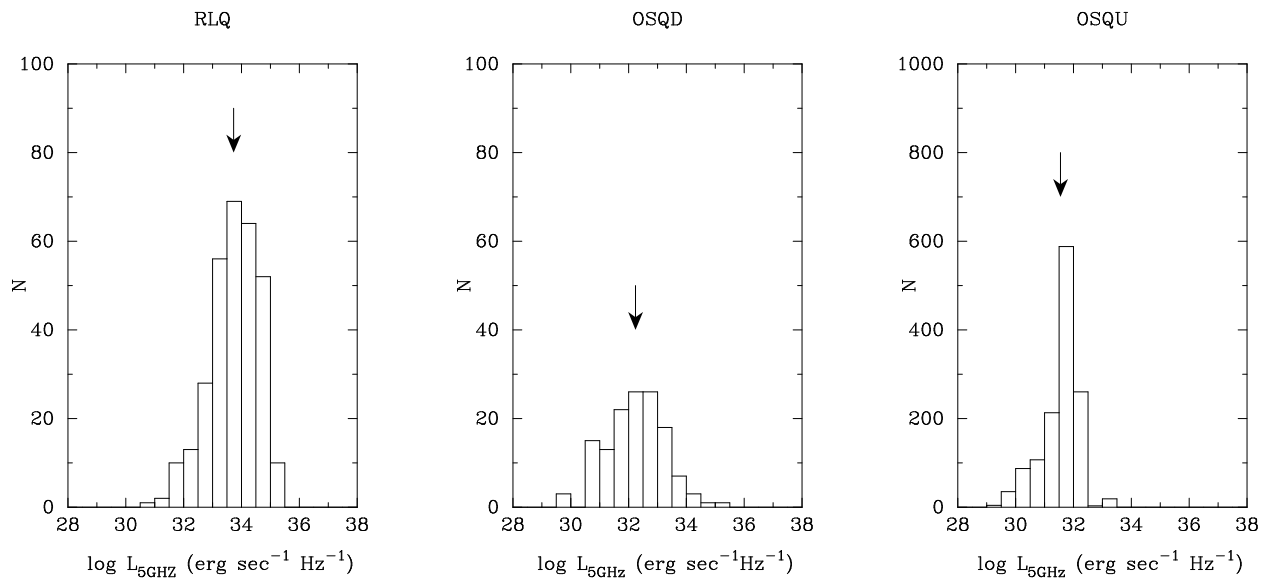


Fig. 6.— Distribution of radio luminosity for the three kinds of quasars. The arrow indicates the mean value.

$$\log R = \log F_r(5 \text{ GHz}) - \log F_{\text{op}}(2500 \text{ \AA}). \quad (6)$$

Figure 7 shows the variation of  $R$  with redshift. There is considerable overlap for  $R \lesssim 3$  between the radio detections and upper limits, but there are only detections at the highest values of  $R$ . There is only one upper limit with  $R > 3$ . At each redshift, there is a maximum to the  $R$  upper limits, and this increases slowly with redshift, so that an envelope is seen. For an upper limit to be found above the envelope, it would be necessary to have quasars at fainter optical magnitudes than are presently to be found in the HB catalogue. In the case of the detections, the maximum value  $R_{\text{max}}(z) = L_{r,\text{max}}(z)/L_{\text{op,min}}(z)$  decreases with redshift. This occurs because the increase in  $L_{r,\text{max}}(z)$  with redshift is slower than the increase in  $L_{\text{op,min}}(z)$  with redshift, as can be seen from Figure 3 and Figure 4. Similarly, the minimum value of  $R$  for the detections,  $R^{\text{min}}(z) = L_{r,\text{min}}(z)/L_{\text{op,max}}(z)$ , increases with redshift, because  $L_{\text{op,max}}(z)$  increases slower than  $L_{r,\text{min}}(z)$ .

Figure 8 shows a histogram of  $\log R$  for radio detections (solid line) and radio upper limits (dashed line). For comparison, the distribution of  $R$  for the radio selected quasars is shown as a dotted line. An important question here is whether the distribution of  $R$  is bimodal. The number of radio detections is not large enough to provide information about the distribution of  $R$  over its wide range. However, as mentioned above, there is considerable overlap in the distributions of the detections and upper limits in the region  $0 \leq R \leq 3$ . It is therefore possible, in principle, to use statistical techniques from the field of survival analysis (see e.g. Feigelson and Nelson 1985) to determine the underlying distribution for a mixed sample of detections and upper limits. If this joint distribution, and the overall distribution of detections have distinct maxima, then one could say that the distribution of  $R$  amongst all quasars is bimodal.

The appropriate technique to derive the joint distribution would be the Kaplan-Meier estimator included as part of the ASURV package (LaValley, Isobe & Feigelson, 1992). One of the requirements of this estimator is that the probability that an object is censored (ie, it has an upper limit), is independent of the value of the censored variable. If such *random censoring* applies to our sample, then the shape of the observed distribution of  $R$  for the detections and upper limits should be the same, in the region of overlap  $0 \leq R \leq 3$ . A Kolmogorov-Smirnov test shows that the two distributions may be considered to be drawn from the same population at only the  $\sim 20$  percent level of significance. Due to the low level of significance it is not possible to use the Kaplan-Meier estimator, or another similar to it, to obtain a joint distribution. A radio survey with a lower limiting flux than FIRST would be needed to convert the upper limits to detections and to constrain the distribution of  $R$  at its lower end. Additional quasars with higher  $R$  values can be found by increasing the area covered by the FIRST survey.

We have mentioned in subsection 3.1 that the separation of the bivariate luminosity function as in Equation 2 is most useful if  $R$  is independent of the optical luminosity. Moreover, such a separation implies that the mean radio luminosity must increase with the optical luminosity. Such

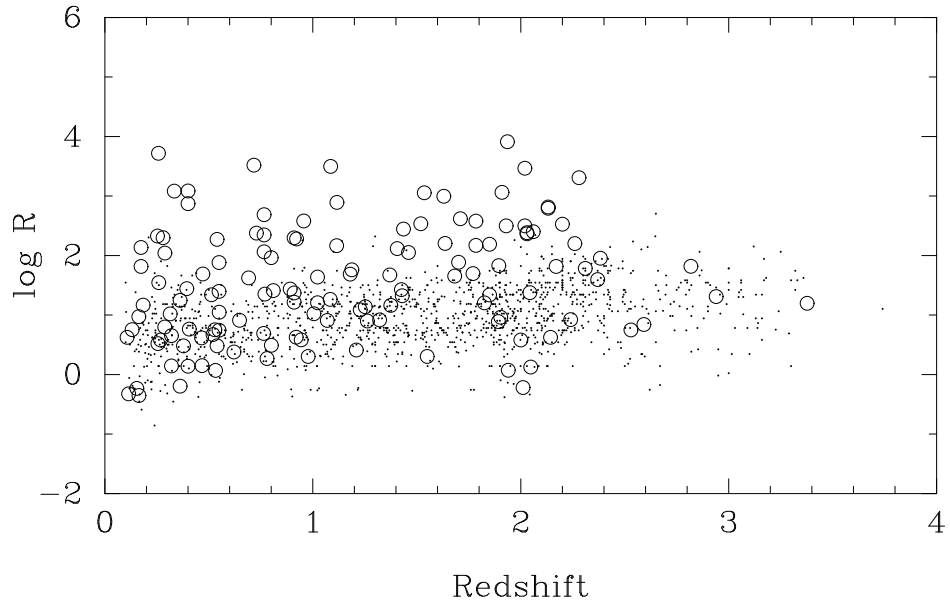


Fig. 7.—  $R = L_r/L_{\text{op}}$  as a function of redshift. Symbols are as in Figure 4

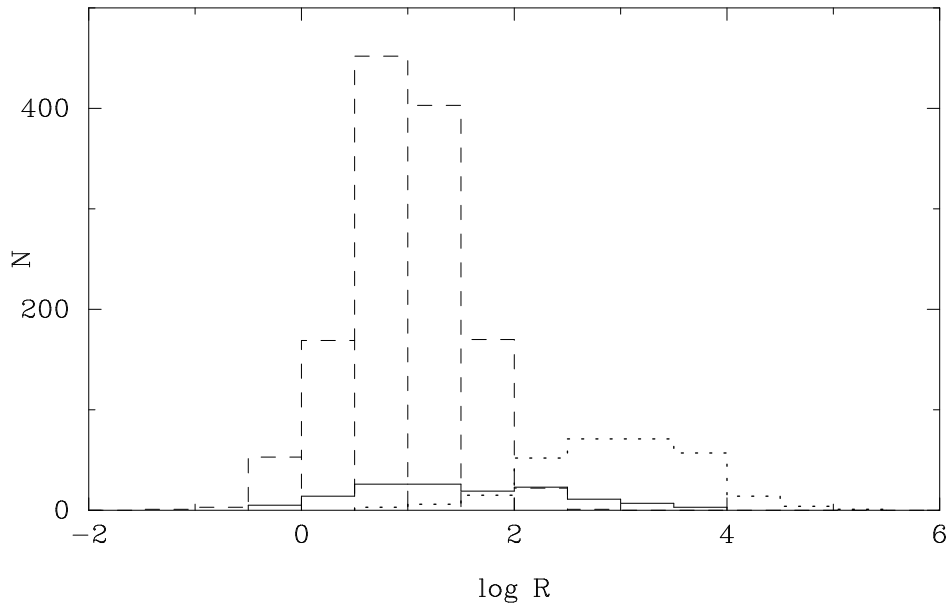


Fig. 8.— Distribution of  $R = L_r/L_{\text{op}}$  for quasars with radio detections (solid line), compared to that for upper limits (dashed line). Radio selected quasars are shown with a dotted line, for comparison.

a correlation between the luminosities is not seen in Figure 5, and as discussed in subsection 3.2,  $L_r$  appears to be distributed independently of  $L_{\text{op}}$  (ie, absolute magnitude). This requires that the distribution of  $R$  depends on  $L_{\text{op}}$  and separation as in Equation 2 is not possible. Separation of the bivariate function as in Equation 1 therefore appears to be the preferred alternative.

#### 4. Radio-loud Fraction

As mentioned in the introduction, the boundary between radio loud and radio quiet quasars can be defined either (1) in terms of a characteristic value of the radio to optical luminosity ratio  $R$ , say  $R = 1$ , or (2) in terms of a characteristic radio luminosity. These two criteria are related to the two ways in which the bivariate luminosity function can be split up between the optical and radio parts as discussed in subsection 3.1. We have found no correlation between the radio and optical luminosities, which implies that a separation involving  $R$ , as in Equation 2 is not consistent with the data. The distribution of  $R$  therefore must be luminosity dependent, and using a single value of  $R$  for separation between radio loud and quiet populations is not appropriate. In this situation, we prefer to adopt the criterion for radio loudness which uses radio luminosity as the discriminant as in MPM90.

The dividing radio luminosity chosen by MPM90, in our units, is  $10^{33.1} \text{ erg sec}^{-1} \text{ Hz}^{-1}$ . This choice was made on the basis of a clear separation between radio detections and upper limits observed by them, which we do not find, as explained in subsection 3.2. We have shown the MPM90 division with a dashed line in Figure 5. It is seen that there is a region below this line with a number of FIRST survey radio detections, but no upper limits. It is therefore possible for us to reduce the dividing luminosity to a level of  $10^{32.5} \text{ erg sec}^{-1} \text{ Hz}^{-1}$ , which is indicated by a solid line in the figure. We define as radio loud all quasars with  $L_r(5 \text{ GHz}) > 10^{32.5} \text{ erg sec}^{-1} \text{ Hz}^{-1}$ , and as radio quiet all quasars below this limit, even though they may have detectable radio emission. The radio loud objects tend to have bright absolute magnitudes, while a dominating fraction of the radio quite detections have  $M_B > -25$ . The faintest of the latter objects could perhaps be active galaxies like Seyferts, which in the local neighborhood are known to have lower radio luminosities than radio galaxies. The radio loud quasars can be considered to be luminous counterparts of the radio galaxies, as in the unification model (Barthel 1989). If the radio loud and quiet classes indeed represent such a physical division, then the host galaxies of the former would perhaps be elliptical, as is the case with radio galaxies, while the hosts of the quiet objects would be disk galaxies like the Seyferts. Deep optical and near-IR imaging of different types of quasars would help in settling this issue.

We have plotted in Figure 9 the variation of radio loud fraction of all quasars as a function of absolute magnitude. The fraction here is taken to be the ratio of the number of radio loud quasars to the number of all non-radio selected quasars in one absolute magnitude wide bin. Each point in Figure 9 is plotted at the centre of the absolute magnitude bin that it represents. The error bar shown is the  $\pm 1\sigma$  deviation about the detected fraction for a random binomial distribution in the

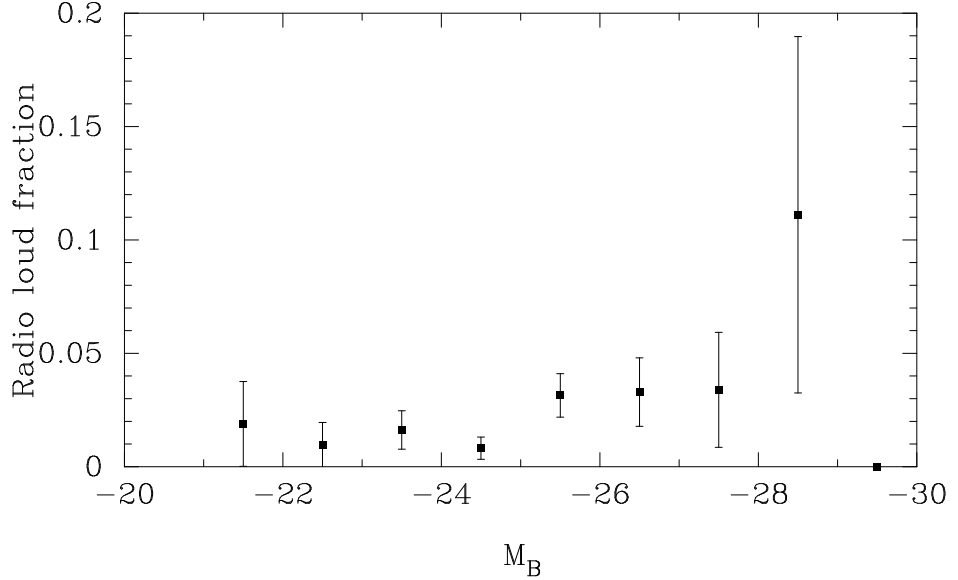


Fig. 9.— Radio loud fraction as a function of absolute magnitude. The error bar shown is the standard deviation for a random binomial distribution in the radio detection fraction.

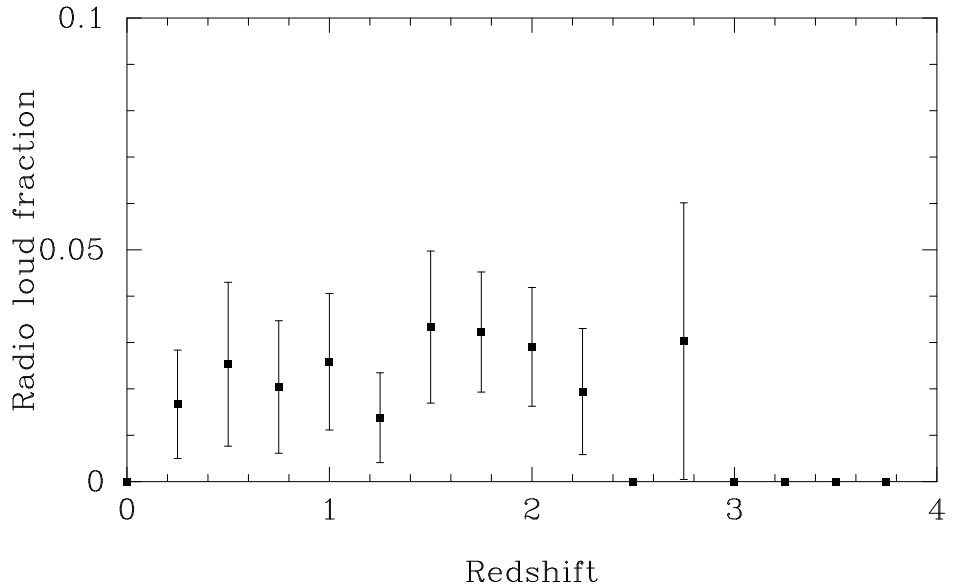


Fig. 10.— Radio loud fraction of quasars as a function of redshift. The error bars are obtained as in Figure 9

radio loud fraction. We find that the radio loud fraction is independent of the absolute magnitude for  $M_B \gtrsim -25$ , while it increases at brighter absolute magnitudes. The reason for this is the increase in radio luminosity towards brighter absolute magnitudes seen in Figure 5, which arises due to the existence of optical and radio flux limits and the consequent redshift dependence of the observed luminosities. An explicit dependence of the radio loud fraction on absolute magnitude would imply a real correlation between the radio and optical luminosities, which is not consistent with the data as we argued in subsection 3.2.

In Figure 10 we have shown the radio loud fraction as a function of redshift. Each point in the figure represents quasars in a bin of width 0.1 in redshift. The error bars are computed as in Figure 9. In contrast with Hooper *et al.* (1996), we do not find a clear peak in the radio loud fraction between a redshift of 0.5 and 1. We find that that the radio loud fraction remains nearly constant upto a redshift of  $z \simeq 2.2$ . There is an indication of increase in the radio loud fraction at higher redshift, but the number of objects here is rather small, as is apparent from the size of the error bars. A very sharp reduction in the radio loud fraction for  $z < 0.5$  was found by BB97. Such a reduction is seen only when radio selected and non-radio selected quasars are considered together, and is also apparent in our data if the two kinds of objects are mixed. We have chosen not to do that, to keep our results free from biases introduced by the radio selected objects, as explained in subsection 3.2.

The large  $1\sigma$  error bars on the plots presented in this section, are caused by the relatively few non-radio selected quasar detections. Due to these error bars it is not possible to distinguish unambiguously between alternatives regarding the dependence of radio loud fraction on other observable properties. More data would be required to confirm or refute our preliminary conclusions regarding the evolution of radio loud fraction with absolute magnitude and redshift.

## 5. Conclusions

The main results of our work are:

- We have reported radio detections of 69 previously undetected quasars.
- We have found additional evidence that the close pair of quasars 1343+266A and 1343+266B are *not* gravitationally lensed.
- We have found no correlation between radio luminosity and optical luminosity for the non-radio selected quasars. Our data is consistent with a bimodal distribution in radio luminosity. The distribution of the ratio of radio to optical luminosity is also bimodal, but this may have little relevance because of the lack of a clear correlation between radio and optical luminosities.

- The radio loud fraction does not seem to be strongly dependent on absolute magnitude, which is consistent with the lack of correlation between radio and optical luminosities.
- The radio loud fraction does not seem to vary significantly with redshift.

The highly heterogeneous nature of the sample used here, makes it inappropriate for studies in parameter ranges where it is seriously incomplete, like high redshift radio quasars. Large surveys like the Digitized Palomar Observatory Sky Survey (DPOSS) and the Sloan Digital Sky Survey (SDSS) will remedy this situation, by providing a large number of quasar candidates for spectroscopic followup.

It is possible that the radio emission from radio loud and radio quiet quasars may be powered by entirely different physical mechanisms. In recent years, there have been suggestions that that radio emission in radio quiet quasars originates in a nuclear starburst rather than accretion onto a central engine (Terlevich *et al.* 1992). A logical step in testing this idea, is to look for differences in the radio and optical morphology of the quasar environment for the two quasar populations (eg. Kellerman 1994). We will report work on the radio morphology of quasar environments obtained from FIRST in a future paper.

We thank R. Srianand for helpful comments and discussion. We thank an anonymous referee whose comments and suggestions helped improve this paper.

This research has made use of the NASA/IPAC Extragalactic Database (NED) which is operated by the Jet Propulsion Laboratory, California Institute of Technology, under contract with the National Aeronautics and Space Administration.

## REFERENCES

Barthel, P. D. 1989, *ApJ*, 336, 606  
Becker, R. H., Gregg, M. D., Hook, I. M., McMahon, R. G., White, R. L. & Helfand, D. J. 1996, *ApJ*, 479, L93  
Becker, R. H., White, R. L., & Helfand, D. J. 1995, *ApJ*, 450, 559  
Bischof, O. B., & Becker, R. H. 1997 (BB97), *AJ*, 113, 2000  
Brinkmann, W., Yuan, W., Siebert, J. 1997, *A&A*, 319, 413  
Crampton, D. *et al.* 1988, *ApJ*, 330, 184  
Cress, C. M., Helfand, D. J., Becker, R. H., Gregg, M. D., & White, R. L. 1996, *ApJ*, 473, 7  
Condon, J. J., Odell, S. L., Puschell, J. J., Stein, W. A. 1981, *ApJ*, 246, 624  
Condon, J. J., Cotton, W. D., Greisen, E. W., Yin, Q. F., Perley, R. A., Taylor, G. B. & Broderick, J. J. 1998, *AJ*, 115, 1693  
Crotts, A. P. S., Bechtold, J., Fang, Y. & Duncan, R. C. 1994, *ApJ*, 437, L79  
Feigelson, E. D. & Nelson, P. I. 1985, *ApJ*, 293, 192 Gregg, M. D. Becker, R. H., White, R. L.,

Helfand, D. J., McMahon, R. G. & Hook, I. M. 1996, AJ, 112, 407  
Havilcek, L. L. & Crain, R. D. 1988, Practical statistics for the physical sciences (Washington DC: American Chemical Society)  
Hewitt A. & Burbidge G. 1993, ApJS, 87, 451  
Hooper, E. J., Impey, C. D., Foltz, C. B. & Hewett, P. C. 1995, ApJ, 445, 62  
Hooper, E. J., Impey, C. D., Foltz, C. B. & Hewett, P. C. 1996, ApJ, 473, 746  
Kellermann, K. I., Sramek, R., Schmidt, M., Shaffer, D. B., & Green, R. 1989, AJ, 98, 1195  
Kellermann, K. I., Sramek, R. A., Schmidt, M., Green, R. F., & Shaffer, D. B. 1994, AJ, 108, 1163  
Kembhavi, A. & Narlikar, J. 1999, Quasars and Active Galactic Nuclei: an Introduction (Cambridge: Cambridge Univ. Press)  
Kukula, M. J., Dunlop, J. S., Hughes, D. H. & Rawlings, S. 1998, MNRAS, 297, 366  
LaValley, M., Isobe, T. & Feigelson, E. 1992, A.S.P. Conference Series, Vol. 25, 245  
Marshall, H.L. 1987, ApJ, 316, 84  
Miller, L., Peacock, J. A., & Mead, A.R.G. 1990, MNRAS, 244, 207  
Monet, D., Bird, A., Canzian, B., Harris, H., Reid, N., Rhodes, A., Sell, S., Ables, H., Dahn, C., Guetter, H., Henden, A., Leggett, S., Levison, H., Luginbuhl, C., Martini, J., Monet, A., Pier, J., Riepe, B., Stone, R., Vrba, F., Walker, R. 1996, USNO-A2.0, (Washington DC: U.S. Naval Observatory)  
Peacock, J. A., Miller, L. & Longair, M. S. 1986, MNRAS, 218, 265  
Sramek, R.A. & Weedman, D.W. 1980, ApJ, 238, 435  
Sandage A. 1965, ApJ, 141, 1560  
Stocke, J. T., Morris, S. L., Weymann, R. J. & Foltz, C. B. 1992, ApJ, 396, 487  
Terlevich, R., Tenorio-Tagle, G., Franco, J. & Melnick, J. 1992, MNRAS, 255, 713  
Veron-Cetty, M.P., & Veron, P. 1991, ESO Scientific Report 10  
Visnovsky, K. L. *et al.* 1992, ApJ, 391, 560  
White, R. L., Becker, R. H., Helfand, D. J., & Gregg, M. D. 1997, ApJ, 475, 479

Table 1. Summary of radio detections

---

---

Number of HB93 quasars in FIRST area:	1704
Number of quasars with radio detections:	389
Number of radio selected quasars:	263
Number of non-radio selected quasars:	126
Number of non-detections:	1315
Percentage of quasars with detected radio emission:	~22%
Percentage of non-radio selected quasars with detected radio emission:	~7%

---

Table 2. FIRST detections of quasars

IAU Designation	Selection Technique	$m_{pg}$	1.4 GHz Peak Radio Flux(mJy)	$z$	Separation (arcsec)	Alternative designation	Recent radio detection
0002-018	O	18.7	62.26	1.71	1.2		
0003-003	R	19.35	3111.27	1.03	0.6	3CR 2	
0004+006	O	17.8	1.55	0.32	1.3		
0009-018	O	18.4	1.61	1.07	2.2	UM 212	
0012-002	O	17.	1.45	1.55	5.0	UM 221	
0012-004	O	18.6	12.67	1.70	0.7		
0013-005	R	20.8	1050.26	1.57	1.6	PKS	
0019+003	O	18.6	1.72	0.31	0.5	A	
0020-020	O	18.4	8.31	0.69	0.4		
0021-010	O	18.2	1.17	0.76	0.7		
0024+003	O	18.0	3.50	1.22	1.7		
0029-018	O	18.7	13.54	2.38	0.3		
0038-020	RX	18.5	593.72	1.17	8.0	PKS	
0038-019	RX	16.86	272.43	1.67	8.4	PKS	
0038-019	RX	16.86	441.62	1.67	8.4	PKS	
0040+005	O	18.	1.09	2.00	2.0	UM 269	
0043+008	OXR	17.	3.04	2.14	1.0	UM 275	
0045-013	O	18.	1.61	2.53	1.3	UM 278	
0045-000	CR	19.4	89.40	1.53	1.4	PKS	
0048+004	O	18.2	13.70	1.18	1.1		
0052-002	O	17.7	3.08	0.64	1.1		
0054-006	R	19.1	114.74	2.77	0.2	PKS	
0056-001	CXR	17.02	2324.98	0.71	0.5	PHL 923	
0059-021	O	18.0	2.37	1.32	0.7		
0100+004	O	19.0	31.65	1.43	4.7		
0101-025	R	19.1	259.45	2.05	3.6	PKS	
0103-021	R	19.84	613.74	2.20	1.4	PKS	
0105-008	R	17.5	883.60	0.31	1.0	PKS	
0107-025	C	18.2	90.65	0.95	2.3	QSO 10	
0112-017	RX	17.41	1025.07	1.36	0.3	PKS	
0122-005	O	18.6	334.34	2.28	1.4	UM 320	
0122-003	R	16.70	1481.35	1.07	0.5	PKS	
0131+009	OR	18.5	8.53	1.37	2.9	UM 338	
0133+004	C	18.5	4.25	0.91	7.1	NGC 622	
0133+004	C	20.2	4.25	1.46	7.1	NGC 622	
0137-018	O	18.5	1.51	2.24	1.9	UM 356	

Table 2—Continued

IAU Designation	Selection Technique	$m_{pg}$	1.4 GHz Peak Flux(mJy)	$z$	Separation (arcsec)	Alternative designation	Recent radio detection
0150-017	O	19.0	35.97	2.02	1.2	UM 375	BB97
0157+001	CX	15.69	22.55	0.16	7.9	MKN 1014	BB97
0157+011	R	18.5	537.75	1.17	1.5	4C 01.05	
0222+000	R	19.	274.34	0.52	1.7	PKS	
0222-008	R	18.4	220.60	0.68	5.9	PKS	
0222-008	R	18.4	813.29	0.68	6.5	PKS	
0225-014	R	18.15	149.85	2.04	2.4	PKS	
0236-015	R	18.80	76.00	1.79	6.9	PKS	
0236-015	R	18.80	115.33	1.79	7.7	PKS	
0240-021	R	19.69	184.75	0.61	0.7	PKS	
0241+011	R	20.	39.25	1.41	2.4	NGC 1073	
0242+009	R	19.60	6.06	1.52	0.5	PKS	
0244-019	C	18.5	26.78	1.78	7.9	US 3148	
0244-019	C	18.5	68.33	1.78	1.3	US 3148	
0244-012	C	16.88	1.13	0.46	9.5	US 3150	
0248-001	C	19.04	53.39	0.76	8.8	US 3224	
0248-001	C	19.04	12.66	0.76	1.3	US 3224	
0248-001	C	19.04	24.34	0.76	7.9	US 3224	
0249+007	C	18.66	7.63	0.47	1.4		
0251-000	C	18.59	7.50	1.68	0.5	US 3293	
0252-002	C	19.61	1.74	1.42	1.2		
0254+007	C	19.53	10.23	1.11	7.4		
0256-021	O	18.5	1.05	0.40	1.0		Hooper <i>et al.</i> 1995
0256-000	O	18.72	2.32	3.37	3.4		
0256-005	R	17.20	5.02	1.99	7.4	PKS	
0256-005	R	17.20	225.85	1.99	5.0	PKS	
0257+004	C	16.71	1.10	0.53	1.4	US 3472	
0259+010	C	19.64	3.15	1.77	2.3		
0300-004	R	18.2	622.14	0.69	1.7	PKS	
0317-023	R	19.5	352.46	2.09	6.3	4C 02.15	
0704+384	R	17.5	66.80	0.57	0.3	4C 38.20	
0711+356	R	18.06	1506.51	1.62	0.9	OI 318	
0714+457	R	...	383.82	0.94	9.2	S4	
0726+431	R	18.5	100.10	1.07	9.0	4C 43.14	
0726+431	R	18.5	160.29	1.07	8.2	4C 43.14	
0729+391	R	18.4	117.16	0.66	0.5	B3	

Table 2—Continued

IAU Designation	Selection Technique	$m_{pg}$	1.4 GHz Peak Radio Flux(mJy)	$z$	Separation (arcsec)	Alternative designation	Recent radio detection
0730+257	R	20.	338.28	2.69	3.1	4C 25.21	
0731+479	R	18.	356.64	0.78	1.2	S4	
0738+313	RX	16.16	2051.49	0.63	0.3	OI 363	
0739+398	R	19.2	375.97	1.70	1.6	B3	
0740+235	R	19.	107.82	0.77	2.7	OI 267	
0740+380	RX	17.6	1113.79	1.06	0.6	3CR 186	
0742+318	R	16.	614.67	0.46	0.4	4C 31.30	
0745+241	R	19.	694.04	0.40	0.4	B2	
0746+483	R	18.5	678.22	1.95	0.6	OI 478	
0748+333	R	18.04	549.70	1.93	0.8	OI 380	
0749+379	R	16.5	11.76	1.20	3.9	UT	
0750+339	R	18.5	43.43	2.07	9.4	UT	
0750+339	R	18.5	17.31	2.07	0.8	UT	
0751+563	O	19.91	1.23	4.28	1.4	PC	
0751+298	R	18.5	398.19	2.10	0.6	4C 29.27	
0752+258	R	18.41	50.12	0.44	5.4	OI 287	
0752+258	R	18.41	234.88	0.44	4.8	OI 287	
0759+341	R	18.5	43.95	2.44	3.9	UT	
0801+303	R	18.5	1031.39	1.44	0.2	4C 30.13	
0804+499	R	17.5	901.70	1.43	1.1	OJ 508	
0805+410	R	19.	589.58	1.42	1.7	UT	
0808+289	R	18.8	39.34	1.88	0.2	B2	
0808+289	R	18.8	15.32	1.88	8.8	B2	
0809+483	RX	17.79	7747.95	0.87	1.0	3CR 196	
0810+327	R	18.	126.85	0.84	0.3	B2	
0810+327	R	18.	62.78	0.84	7.5	B2	
0812+367	R	18.	645.65	1.02	2.3	OJ 320	
0812+332	R	18.	327.89	2.42	0.0	B2	
0814+350	R	20.0	6.28	1.34	0.1		
0814+227	R	18.	42.17	0.98	2.5	4C 22.20	
0814+425	U	18.5	944.26	0.25	0.2	OJ 425	
0820+225	R	19.2	1919.32	0.95	0.7	PKS	
0820+560	R	18.0	1363.46	1.41	0.3	OJ 535	
0821+394	R	18.5	1403.96	1.21	0.5	4C 39.23	
0821+447	R	18.1	430.56	0.90	3.9	4C 44.17	
0822+272	C	17.7	94.61	2.06	1.8	W1	

Table 2—Continued

IAU Designation	Selection Technique	$m_{pg}$	1.4 GHz Peak Radio Flux(mJy)	$z$	Separation (arcsec)	Alternative designation	Recent radio detection
0824+355	R	20.5	913.49	2.24	0.6	4C 35.20	
0827+243	RX	17.26	835.48	0.93	0.3	OJ 248	
0827+378	R	18.11	2032.16	0.91	0.1	4C 37.24	
0829+337	R	18.5	211.57	1.10	7.0	B2	
0831+349	R	19.2	18.30	1.40	0.2		
0832+251	C	...	1.84	0.32	7.3	PG	
0833+276	R	...	300.48	0.76	6.3	OJ 256	
0833+446	C	15.51	9.39	0.25	1.5	US 1329	BB97
0834+250	R	18.	422.63	1.12	0.1	OJ 259	
0838+456	C	17.39	65.53	1.40	3.7	US 1498	BB97
0841+495	C	19.	74.55	2.13	1.4	NGC 2639	
0841+495	C	19.	70.89	2.13	6.2	NGC 2639	
0841+449	O	20.9	1.30	2.17	9.5		
0843+349	RX	18.5	39.54	1.57	0.1		
0843+349	RX	18.5	16.74	1.57	7.3		
0844+446	R	...	6.29	0.46	6.7	55W 179	
0849+336	C	17.4	1.19	0.62	9.2	NGC 2683	
0849+336	C	18.7	1.19	1.26	9.2	NGC 2683	
0849+336	C	19.3	1.19	1.25	9.2	NGC 2683	
0850+284	X	17.7	71.73	0.92	5.1	1E	
0853+515	C	19.5	4.36	2.31	7.1	NGC 2693	BB97
0859+470	R	18.7	1655.19	1.46	1.6	4C 47.29	
0901+285	R	17.6	34.28	1.12	0.3	B2	
0904+386	R	18.5	39.73	1.74	5.2	UT	
0904+386	R	18.5	44.26	1.74	2.2	UT	
0904+386	R	18.5	24.38	1.74	9.9	UT	
0906+430	RX	18.48	3444.11	0.67	0.2	3CR 216	
0907+381	R	18.	250.93	2.16	1.7	UT	
0910+392	R	19.0	23.71	0.63	1.2	B3	
0910+392	R	19.0	7.13	0.63	4.1	B3	
0913+391	R	18.5	967.97	1.25	0.0	B3	
0913+391	R	20.	967.97	1.26	1.2	4C 38.28	
0917+449	R	19.	1079.25	2.18	0.5	S4	
0918+381	R	18.8	42.90	1.10	3.3	B3	
0920+313	R	18.	251.68	0.89	1.4	B2	
0923+392	RX	17.86	2752.50	0.69	0.3	4C 39.25	

Table 2—Continued

IAU Designation	Selection Technique	$m_{pg}$	1.4 GHz Peak Radio Flux(mJy)	$z$	Separation (arcsec)	Alternative designation	Recent radio detection
0924+301	U	21.	52.82	2.02	1.1		
0926+388	R	18.5	138.83	1.63	0.7	B3	
0927+362	R	19.	975.97	1.15	4.1	3CR 220.2	
0927+362	R	19.	749.85	1.15	3.5	3CR 220.2	
0928+312	R	18.6	126.86	1.31	2.9	B2	
0928+349	R	19.8	38.65	0.92	0.8		
0928+348	R	20.3	11.22	2.30	0.4		
0928+348	R	20.3	2.66	2.30	8.3		
0932+367	R	18.5	283.00	2.84	1.7	UT	
0935+430	C	18.83	3.16	2.04	1.0	US 795	BB97
0937+391	R	18.	41.28	0.61	6.4	4C 39.27	
0938+450	C	18.7	13.81	0.80	1.1	US 844	BB97
0941+522	R	18.6	628.01	0.56	2.1	OK 568	
0941+261	R	18.7	730.69	2.91	0.6	OK 270	
0945+436	C	17.78	2.72	1.89	0.3	US 987	BB97
0945+408	R	17.5	1439.97	1.25	0.7	4C 40.24	
0949+363	R	18.5	99.80	2.05	1.7	UT	
0952+441	C	17.28	2.30	0.46	1.0	US 1101	
0952+457	C	16.76	31.38	0.25	2.7	US 1107	Brinkmann <i>et al.</i> 19
0952+357	R	18.5	190.74	1.24	4.7	4C 35.21	
0953+254	RX	17.13	1041.77	0.71	0.2	OK 290	
0954+556	R	17.7	2804.17	0.90	5.0	PKS	
0955+387	R	20.0	161.59	1.40	0.2	B3	
0955+476	R	18.	763.01	1.87	3.9	OK 492	
0955+326	RX	15.78	1204.19	0.53	0.6	TON 469	
0957+561	R	17.25	283.96	1.41	3.7	A	
0957+561	R	17.35	283.96	1.41	7.4	B	
1001+226	R	18.	33.93	0.97	0.9	4C 22.26	
1007+417	R	16.5	258.74	0.61	1.1	4C 41.21	
1009+334	R	17.5	172.71	2.26	2.0	UT	
1010+350	R	19.8	348.65	1.41	0.4	B2	
1011+250	CXR	15.4	500.27	1.63	1.0	TON 490	
1011+280	R	18.6	82.99	0.89	4.1	4C 28.25	
1011+280	R	18.6	241.63	0.89	5.2	4C 28.25	
1012+232	R	17.5	673.56	0.56	0.5	4C 23.24	
1015+277	R	17.5	844.36	0.46	8.7	B2	

Table 2—Continued

IAU Designation	Selection Technique	$m_{pg}$	1.4 GHz Peak Radio Flux(mJy)	$z$	Separation (arcsec)	Alternative designation	Recent radio detection
1015+359	R	19.	571.31	1.22	4.8	OL 326	
1015+383	R	18.	5.39	0.38	7.0	UT	
1018+348	R	17.75	317.10	1.40	0.6	OL 331	
1019+309	R	16.75	907.01	1.31	0.5	OL 333	
1020+400	R	17.5	807.88	1.25	1.5	UT	
1028+313	RX	16.71	57.04	0.17	6.4	B2	
1028+313	RX	16.71	58.74	0.17	0.3	B2	
1030+415	R	18.2	406.68	1.12	3.1	VR10.	
1038+528	R	17.4	414.78	0.67	0.3	OL 564	
1038+528	R	18.5	101.76	2.29	0.1	B	
1042+349	R	18.5	40.45	2.34	0.3		
1044+476	R	18.4	734.01	0.80	1.4	OL 474	
1045+350	R	20.8	17.23	0.92	0.3		
1048+347	R	20.45	540.40	2.52	2.9	B2	
1048+240	R	18.5	282.73	1.27	7.9	4C 24.23	
1048+240	R	18.5	110.43	1.27	7.0	4C 24.23	
1050+542	R	18.2	117.86	1.00	6.5		
1050+542	R	18.2	51.44	1.00	5.4		
1055+499	R	19.5	225.14	2.39	0.2	5C2.5	
1059+282	R	19.	240.69	1.86	0.6	GC	
1105+392	R	18.5	603.57	0.78	0.7	B3	
1105+392	R	18.5	22.78	0.78	7.4	B3	
1109+357	X	18.1	4.29	0.91	6.1	1E	
1109+350	R	18.5	181.57	1.94	0.1	UT	
1111+408	RX	17.98	1740.12	0.73	1.6	3CR 254	
1115+536	R	18.4	612.32	1.23	3.0	OM 525	
1115+536	R	18.4	266.32	1.23	5.7	OM 525	
1115+407	CX	16.02	1.04	0.15	5.5	PG	
1123+441	R	19.1	87.92	0.48	0.9	W1	
1123+264	R	17.5	904.38	2.34	0.1	PKS	
1123+434	R	18.4	24.75	2.01	2.0	W1	
1124+571	R	19.0	473.93	2.89	2.4	OM 540/4	
1124+271	C	17.0	2.18	0.37	2.9	US 2450	BB97
1128+315	C	16.53	121.84	0.28	3.2	B2	
1130+284	C	17.52	9.73	0.51	1.9	US 2599	BB97
1132+303	R	18.24	306.09	0.61	0.6	3C 261	

Table 2—Continued

IAU Designation	Selection Technique	$m_{pg}$	1.4 GHz Peak Flux(mJy)	$z$	Separation (arcsec)	Alternative designation	Recent radio detection
1132+303	R	18.24	286.52	0.61	8.0	3C 261	
1134+349	R	19.2	23.41	0.83	0.6		
1145+321	C	17.14	15.76	0.54	9.5	US 2978	BB97
1145+321	C	17.14	48.24	0.54	0.6	US 2978	BB97
1145+321	C	17.14	3.51	0.54	9.7	US 2978	BB97
1146+562	R	19.2	21.88	0.95	4.3	W1	
1147+339	R	18.5	98.64	1.49	0.4	UT	
1148+568	R	20.5	83.16	1.78	0.7	W1	
1148+477	R	18.0	143.90	0.86	2.2	4C 47.33	
1148+549	CR	15.82	4.30	0.97	0.8	PG	
1148+387	R	17.04	391.60	1.30	1.2	4C 38.31	
1150+497	CR	17.50	548.11	0.33	0.0	LB 2136	
1153+534	R	20.3	8.03	1.75	1.9	W1	
1153+317	R	18.96	2833.64	1.55	0.3	4C 31.38	
1156+295	CR	14.41	1855.80	0.72	0.1	4C 29.45	
1157+532	R	19.7	129.83	1.99	0.7	W2	
1204+399	R	18.5	235.09	1.33	2.2	UT	
1204+281	R	18.1	596.14	2.17	2.1	B2	
1206+439	R	18.42	1439.20	1.39	4.6	3CR 268.4	
1206+439	R	18.42	419.00	1.39	4.8	3CR 268.4	
1207+398	R	19.4	23.04	2.33	1.2	W3	
1208+322	R	16.	19.15	0.38	2.5	B2	
1211+334	R	17.89	1372.84	1.59	8.4	ON 319	
1213+350	R	20.1	1323.86	0.85	0.3	4C 35.28	
1214+348	R	18.7	154.45	2.64	0.6		
1214+474	R	19.2	94.56	1.10	0.0	W2	
1215+333	R	17.5	183.25	2.60	0.6	GC	
1216+487	R	18.5	659.98	1.07	1.2	ON 428	
1218+339	R	18.61	586.79	1.51	4.5	3CR 270.1	
1218+339	R	18.61	1929.95	1.51	3.8	3CR 270.1	
1220+373	R	18.6	24.36	0.48	0.1	B2	
1222+228	CXR	15.49	3.86	2.04	0.1	TON 1530	
1223+252	CXR	16.	6.87	0.26	0.6	TON 616	
1225+317	RX	15.87	315.34	2.21	1.8	B2	
1229+405	R	19.0	46.38	0.64	7.7	B3	
1229+405	R	19.0	186.72	0.64	2.7	B3	

Table 2—Continued

IAU Designation	Selection Technique	$m_{pg}$	1.4 GHz Peak Radio Flux(mJy)	$z$	Separation (arcsec)	Alternative designation	Recent radio detection
1231+349	R	19.3	5.85	0.84	0.2		
1231+294	C	16.	1.09	2.01	3.9	CSO 151	
1234+335	R	18.5	175.82	1.28	2.2	UT	
1234+265	O	21.6	3.50	2.20	3.3		BB97
1240+381	R	19.	536.82	1.31	0.7	B2	
1244+324	R	17.2	77.07	0.94	1.4	4C 32.41	
1247+450	R	17.8	338.17	0.79	7.3	4C 45.26	
1248+350	R	20.0	240.73	0.97	0.3		
1250+568	RX	17.93	2258.50	0.32	1.2	3CR 277.1	
1250+313	O	16.7	1.76	0.78	0.2	LB 11408	
1251+398	R	19.2	30.40	2.10	0.9	B3	
1254+370	CR	17.84	65.93	0.28	0.4	B 142	
1256+357	CXR	18.24	15.55	1.89	0.9	B 194	
1257+346	CR	16.99	10.56	1.37	0.5	B 201	
1258+287	RX	17.38	192.10	0.64	2.9	5C4.1	
1258+404	R	19.44	269.63	1.66	6.3	3CR 280.1	
1258+286	RX	19.	78.54	1.37	4.3	5C4.1	
1258+342	OR	19.	35.99	1.93	5.9	KP 33	
1301+295	CR	18.9	42.80	1.51	5.8	5C4.1	
1305+364	CR	18.01	1.20	0.92	0.8	B 330	
1306+274	R	18.5	92.39	1.53	8.1	OP 211	
1306+274	R	18.5	116.88	1.53	2.0	OP 211	
1308+284	O	18.1	1.23	0.52	4.2	US 370	
1308+297	O	17.4	10.82	1.85	1.1		BB97
1309+378	CR	17.65	1.20	0.54	0.6	B 503	
1309+355	CR	15.45	43.92	0.18	0.2	PG	
1315+346	R	19.	420.95	1.05	0.4	OP 326	
1315+346	R	19.	29.61	1.05	4.1	OP 326	
1315+473	O	18.01	1.97	2.59	3.6	PC	BB97
1316+269	O	21.0	20.84	1.91	1.5		BB97
1316+270	O	20.0	7.22	2.26	3.9		BB97
1317+380	R	18.6	131.81	0.83	3.5	B3	
1317+380	R	18.6	70.96	0.83	6.5	B3	
1317+520	R	17.	297.21	1.05	2.8	4C 52.27	
1328+254	RX	17.67	6826.39	1.05	0.0	3CR 287	
1328+307	RX	17.25	14777.9	0.84	0.2	3CR 286	

Table 2—Continued

IAU Designation	Selection Technique	$m_{pg}$	1.4 GHz Peak Flux(mJy)	$z$	Separation (arcsec)	Alternative designation	Recent rad detection
1332+552	R	16.	9.88	1.25	0.9	4C 55.27	
1333+459	R	18.5	262.72	2.45	0.2	S4	
1333+277	O	19.4	61.56	1.11	4.6		
1334+246	U	15.	19.18	0.10	0.2		
1335+283	O	20.4	98.85	1.08	0.5		
1336+351	R	20.0	104.72	1.54	2.5		
1338+394	R	19.0	14.92	0.58	5.4	B3	
1338+394	R	19.0	18.12	0.58	6.5	B3	
1339+287	R	18.6	1.54	0.33	1.8		
1340+287	R	18.35	65.57	1.03	1.5	B2	
1340+289	R	17.07	217.37	0.90	1.5	B2	
1342+264	O	18.6	8.03	1.18	5.4		BB97
1342+389	R	17.5	159.53	1.53	4.7	B3	
1343+267	O	19.8	1.49	0.89	4.2		
1343+266	O	20.23	8.90	2.03	7.4	A Crotts <i>et al.</i> 1994	
1343+266	O	20.18	8.90	2.03	2.1	B Crotts <i>et al.</i> 1994	
1343+386	R	18.5	845.79	1.84	0.6	4C 38.37	
1344+264	O	19.1	1.66	1.82	6.9		
1347+539	R	17.3	960.41	0.97	1.2	4C 53.28	
1348+384	R	18.	77.34	1.39	0.1	UT	
1348+384	R	18.	32.95	1.39	8.5	UT	
1348+392	R	19.0	130.30	1.58	0.5	B3	
1351+267	R	17.18	22.35	0.31	1.1	B2.2	
1351+318	R	17.4	74.13	1.32	4.0	B2	
1351+318	R	17.4	76.61	1.32	4.9	B2	
1353+306	R	18.2	123.06	1.01	0.9	B2	
1354+258	R	18.5	173.68	2.00	3.7	OP 291	
1402+436	U	16.5	1.59	0.32	1.2	CSO 409	
1402+261	CXR	15.57	1.19	0.16	8.1	PG	
1407+265	CXR	15.73	8.85	0.94	0.7	PG	
1409+344	R	18.5	41.68	1.82	7.9	UT	
1409+344	R	18.5	92.49	1.82	2.7	UT	
1413+373	R	18.	406.30	2.36	3.7	UT	
1414+347	R	18.	60.69	0.75	8.2	UT	
1414+347	R	18.	31.71	0.75	3.6	UT	
1415+451	C	15.74	1.09	0.11	1.7	PG	

Table 2—Continued

IAU Designation	Selection Technique	$m_{pg}$	1.4 GHz Peak Flux(mJy)	$z$	Separation (arcsec)	Alternative designation	Recent radio detection
1415+463	R	17.9	696.65	1.55	0.4	4C 46.29	
1417+385	R	19.3	651.90	1.83	0.7	UT	
1419+315	R	20.90	78.08	1.54	8.5	B2	
1419+315	R	20.90	81.43	1.54	0.7	B2	
1419+315	R	20.90	104.24	1.54	7.7	B2	
1421+330	C	16.70	8.71	1.90	0.4	MKN 679	
1421+359	R	17.5	71.37	1.57	2.4	UT	
1422+231	R	16.5	273.42	3.62	0.4		
1423+242	R	17.2	394.80	0.64	9.6	4C 24.31	
1423+242	R	17.2	121.14	0.64	1.2	4C 24.31	
1425+267	CXR	15.68	1.55	0.36	8.5	TON 202	
1425+267	CXR	15.68	42.72	0.36	0.3	TON 202	
1426+295	R	18.5	402.07	1.42	0.8	B2	
1435+315	R	18.	13.94	1.36	3.3	B2	
1435+315	R	18.	60.37	1.36	1.0	B2	
1435+383	R	18.	180.04	1.61	1.9	UT	
1435+248	RX	19.	252.95	1.01	1.0	4C 24.32	
1435+355	R	18.	14.97	0.54	9.3	UT	
1435+355	R	18.	16.53	0.54	4.5	UT	
1441+522	R	19.97	1008.23	1.57	5.3	3C 303C	
1444+417	R	18.2	73.98	0.67	3.6	B3	
1452+301	R	18.5	650.82	0.58	2.2	OQ 287	
1455+348	R	20.0	231.69	2.73	0.1		
1506+339	R	18.5	130.95	2.20	1.2	UT	
1512+370	RX	15.5	48.97	0.37	0.3	4C 37.43	
1520+344	R	19.	176.03	1.31	2.2	UT	
1522+259	C	18.79	1.54	0.55	0.7	LB 9695	
1525+314	R	19.1	792.83	1.38	7.2	B2	
1525+227	CXR	16.39	267.42	0.25	4.6	LB 9743	
1538+477	CR	16.01	40.36	0.77	0.9	PG	
1541+355	R	19.5	120.89	1.70	1.3	UT	
1542+373	R	17.7	602.99	0.97	0.9	4C 37.45	
1543+489	C	16.05	2.38	0.40	4.0	PG	
1546+353	R	18.	140.94	0.48	1.5	UT	
1555+332	RX	18.3	77.06	0.94	1.0	GC	
1556+335	RX	17.	142.96	1.65	0.2	GC	

Table 2—Continued

IAU Designation	Selection Technique	$m_{pg}$	1.4 GHz Peak Radio Flux(mJy)	$z$	Separation (arcsec)	Alternative designation	Recent radio detection
1605+355	R	18.	97.91	0.97	2.7	UT	
1606+289	RX	19.	3.35	1.98	3.5	4C 28.40	
1611+343	RX	17.76	3532.04	1.40	0.5	DA 406	
1612+378	R	18.5	93.29	1.63	7.6	UT	
1612+378	R	18.5	46.53	1.63	6.5	UT	
1612+261	CXR	15.41	17.69	0.13	0.5	TON 256	
1620+356	R	18.5	177.51	1.47	9.2	4C 35.41	
1620+356	R	18.5	10.79	1.47	2.2	4C 35.41	
1621+392	R	17.5	189.57	1.97	1.9	UT	
1621+361	R	18.5	259.58	0.87	1.4	UT	
1622+238	RX	17.47	635.34	0.92	7.8	3CR 336	
1622+238	RX	17.47	101.74	0.92	4.1	3CR 336	
1622+395	R	17.5	76.71	1.12	5.4	UT	
1622+395	R	17.5	132.32	1.12	3.5	UT	
1623+269	RX	17.5	368.12	0.77	1.3	4C 26.48	
1624+416	R	22.	1694.61	2.55	0.0	4C 41.32	
1624+349	R	19.4	26.35	1.33	0.8		
1628+380	O	17.0	20.00	0.39	1.1		
1628+363	R	17.5	149.78	1.25	5.4	4C 36.28	
1628+363	R	17.5	52.46	1.25	1.0	4C 36.28	
1628+363	R	17.5	211.31	1.25	9.7	4C 36.28	
1629+439	R	18.5	581.05	1.16	0.9	4C 43.39	
1631+373	O	18.6	3.37	2.94	1.3		
1631+395	O	16.7	41.29	1.02	0.1		
1631+395	O	16.7	15.24	1.02	8.8		
1632+391	R	18.	915.40	1.08	0.6	4C 39.46	
1633+382	RX	18.1	2653.87	1.81	1.8	GC	
1634+269	R	17.75	17.29	0.56	7.4	PKS	
1636+473	R	...	601.81	0.74	8.8	4C 47.44	
1638+398	R	18.5	1088.22	1.66	1.5	NRAO 512	
1640+396	XR	18.3	40.63	0.54	6.6		
1640+401	XR	17.1	6.89	1.00	8.7		
1641+399	RX	15.96	6050.06	0.59	0.4	3CR 345	
1656+348	R	19.	406.35	1.93	0.3	OS 392	
1656+571	R	17.4	817.61	1.28	1.5	4C 57.28	
1656+477	R	18.0	873.76	1.62	0.1	S4	

Table 2—Continued

IAU Designation	Selection Technique	$m_{pg}$	1.4 GHz Peak Flux(mJy)	$z$	Separation (arcsec)	Alternative designation	Recent radio detection
1657+265	R	18.	391.07	0.79	1.3	4C 26.51	
1700+518	C	15.43	19.20	0.28	0.9	PG	
1701+379	R	19.	83.11	2.45	6.5	UT	
1702+298	R	19.14	1200.93	1.93	0.3	4C 29.50	
1705+456	R	17.6	681.65	0.64	0.7	4C 45.34	
1705+456	R	17.6	10.17	0.64	8.3	4C 45.34	
1710+329	R	19.	167.28	1.96	1.4	UT	
1713+504	R	...	44.92	1.09	9.5	53W 009	
1714+502	R	...	47.66	1.12	9.7	53W 015	
1715+535	CR	16.30	1.62	1.94	4.4	PG	
1718+481	CR	15.33	61.37	1.08	0.6	PG	
1719+357	R	...	386.51	0.26	3.4	B2	
1719+497	R	...	97.24	2.15	7.3	53W 075	
1719+348	R	21.1	55.23	1.83	0.5		
1720+499	R	...	10.15	0.54	8.4	53W 080	
1720+499	R	...	7.25	0.54	7.4	53W 080	
1720+499	R	...	5.27	1.82	6.2	53W 085	
1721+343	RX	16.5	438.57	0.20	0.5	4C 34.47	
1724+399	R	18.	475.49	0.66	0.8	UT	
1726+344	R	18.5	72.17	2.42	0.8	UT	
1727+386	R	17.5	240.27	1.39	1.8	UT	
1729+491	R	18.8	782.21	1.03	0.4	4C 49.29	
1729+501	R	17.7	50.10	1.10	0.6	4C 50.43	
1738+499	R	19.	409.90	1.54	0.3	OT 463	
1739+522	RX	18.5	1508.16	1.37	1.5	4C 51.37	
2131-009	XR	21.6	10.30	1.63	0.8		
2134+004	CXR	17.55	3546.71	1.93	0.9	PHL 61	
2211+006	O	19.23	18.31	0.91	6.3	PC	
2227-088	R	17.5	952.78	1.56	0.5	PKS	
2231-008	O	17.6	1.07	1.20	1.4		
2235+009	O	18.5	1.02	0.52	1.0		
2245-009	O	17.4	1.54	0.80	1.7		
0041+001	R	19.28	108.53	1.12	0.0	PKS	
0742+333	R	17.7	98.52	0.61	0.2	GC	
0952+338	C	17.	35.73	2.50	0.1	CSO 239	
1255+370	R	17.8	690.34	0.28	0.8	B2	

Table 2—Continued

IAU Designation	Selection Technique	$m_{pg}$	1.4 GHz Peak Radio Flux(mJy)	$z$	Separation (arcsec)	Alternative designation	Recent radio detection
1339+274	O	19.0	238.13	1.18	0.3		
1343+284	O	18.0	5.83	0.65	0.2		
1420+326	R	17.5	412.83	0.68	0.2	OQ 334	
1623+268	O	17.3	10.12	2.52	0.2	KP 77	

<sup>a</sup>Selection Technique O:Objective Prism R: Radio C: UV-Excess X: X-Ray U: Selection technique not mentioned.